Monthly Notices
of the
ROYAL ASTRONOMICAL SOCIETY

Mon. Not. R. Astron. Soc. **427,** 2881–2888 (2012) doi:10.1111/j.1365-2966.2012.22123.x

The C IV Baldwin effect in quasi-stellar objects from Seventh Data Release of the Sloan Digital Sky Survey

Wei-Hao Bian,[1⋆] Li-Ling Fang,[1] Ke-Liang Huang[1] and Jian-Min Wang[2]

[1] *Department of Physics and Institute of Theoretical Physics, Nanjing Normal University, Nanjing 210097, China*
[2] *Key Laboratory for Particle Astrophysics, Institute of High Energy Physics, Chinese Academy of Sciences, Beijing 100039, China*

Accepted 2012 September 12. Received 2012 September 10; in original form 2012 April 30

ABSTRACT

Using the properties of the quasi-stellar object (QSO) catalogue of Shen et al., from the Seventh Data Release of the Sloan Digital Sky Survey, we investigate the Baldwin effect, its slope evolution, and the underlying drive for a large sample of 35 019 QSOs with reliable spectral analysis. We find that the Baldwin effect exists in this large sample of QSOs, and that it is almost the same in 11 different redshift bins, up to $z \sim 5$. The slope is -0.238 using the bivariate correlated errors and intrinsic scatter (BCES) algorithm – the equivalent width (EW) of C IV depends on the continuum – and -0.787 using the BCES bisector. For 11 redshift bins, there is an increase in the slope of the Baldwin effect from $z \sim 1.5$ to $z \sim 2.0$. From $z \sim 2.0$ to $z \sim 5.0$, the change in the slope is not clear, considering the uncertainties or larger redshift bins. There is a strong correlation between the rest-frame C IV EW and the C IV-based $M_{\rm BH}$, while the relation between the C IV EW and the Mg II-based $M_{\rm BH}$ is very weak. With the correction of the C IV-based $M_{\rm BH}$ from the C IV blueshift relative to Mg II, we suggest that this strong correlation is a result of the bias of the C IV-based $M_{\rm BH}$, with respect to that from the Mg II line. Considering the Mg II-based $M_{\rm BH}$, a medium strong correlation is found between the C IV EW and the Eddington ratio, which implies that the Eddington ratio seems to be a better underlying physical parameter than the central black hole mass.

Key words: black hole physics – galaxies: active – quasars: emission lines.

1 INTRODUCTION

Broad emission lines are a prominent property of quasi-stellar objects (QSOs). Baldwin (1977) was the first to discover an anti-correlation between the equivalent width (EW) of the C IV λ1549 emission line and its nearby continuum luminosity in the QSO rest frame (i.e. the Baldwin effect; see a review by Shields 2007). Over the past 30 yr, there has been a significant effort to confirm this effect in C IV, including other prominent emission lines (e.g. Lyα, C III, Si IV, Mg II, [O III], Fe Kα), as well as to explore its origin and evolution (e.g. Dietrich et al. 2002; Zhou & Wang 2005; Kong et al. 2006; Netzer et al. 2006; Xu et al. 2008; Wu et al. 2009; Richards et al. 2011).

Although it is believed that the Baldwin effect exists for many ultraviolet/optical emission lines, its origin is a problem that is still debated. Several interpretations about its origin have been proposed (e.g. Netzer, Laor & Gondhalekar 1992; Dietrich et al. 2002; Shang et al. 2003; Baskin & Laor 2004; Xu et al. 2008; Wu et al. 2009). One promising interpretation is the softening of the spectral energy distribution (SED) for increasing luminosity, which lowers the ion populations that have high ionization potentials (e.g. Netzer et al. 1992; Dietrich et al. 2002).

With the progress that has been made in our understanding of the virial mass of a supermassive black hole (SMBH; $M_{\rm BH}$), it is possible to explore the underlying physical parameters for the origin of the C IV Baldwin effect, such as the Eddington ratio (i.e. the ratio of the bolometric luminosity to the Eddington luminosity, $L_{\rm Bol}/L_{\rm Edd}$), the $M_{\rm BH}$ and the luminosity dependence of metallicity (e.g. Dietrich et al. 2002; Shang et al. 2003; Baskin & Laor 2004, 2005; Warner, Hamann & Dietrich 2004; Xu et al. 2008). The single-epoch virial mass $M_{\rm BH}$ can be calculated from the broad linewidth (e.g. Hβ, Hα, Mg II, C IV) and empirical luminosity–size relation (e.g. Kaspi et al. 2000; Bian & Zhao 2004; Vestergaard & Peterson 2006; Shen et al. 2011). The bolometric luminosity $L_{\rm Bol}$ can be calculated from the monochromatic luminosity using the correction factor estimated from the composite SED (e.g. Richards et al. 2006; Shen et al. 2011).

For the Palomar–Green (PG) sample of QSOs, Baskin & Laor (2004) have found a strong correlation between the C IV EW and $L_{\rm Bol}/L_{\rm Edd}$, and they have suggested that $L_{\rm Bol}/L_{\rm Edd}$ is the primary physical parameter driving the Baldwin effect. However, Shang et al. (2003) have used the spectral principal component (SPC) method and have found that there is no correlation between the Baldwin

⋆E-mail: whbian@njnu.edu.cn

effect and $L_{\rm Bol}/L_{\rm Edd}$ or $M_{\rm BH}$ as underlying physical parameters. Nikolajuk & Walter (2012) have found that weak-line QSOs do not follow the relation between the C IV EW and $L_{\rm Bol}/L_{\rm Edd}$ given by Baskin & Laor (2004). However, these weak-line QSOs have the same X-ray–optical spectral index ($\alpha_{\rm ox}$), with respect to other normal QSOs. It has been suggested that weak-line QSOs are caused by a possible low covering factor (Nikolajuk & Walter 2012).

In the past, most studies have used relatively small samples. The Sloan Digital Sky Survey (SDSS) has made it possible for us to investigate the Baldwin effect using a larger sample of QSOs (e.g. Xu et al. 2008; Richards et al. 2011). With the SDSS Fifth Data Release (DR5), Xu et al. (2008) used the result from the pipeline of the SDSS spectral fit, which measured the line feature using a single Gaussian fit for the continuum subtracted spectrum. They found that, up to $z \approx 5$, the slope of the Baldwin effect seems to have no effect on cosmological evolution. They also found that the C IV EW has a stronger correlation with the C IV-based $M_{\rm BH}$ than $L_{\rm Bol}/L_{\rm Edd}$, suggesting that $M_{\rm BH}$ is probably the primary drive for the Baldwin effect.

Recently, Shen et al. (2011) have made a careful spectral analysis and have provided a compilation of properties for 105 783 QSOs from the SDSS DR7 QSO catalogue. Here, we use their data to reinvestigate the Baldwin effect for the C IV line and its origin. We is briefly describe our adopted sample in Section 2, and we give the results and analysis in Section 3. We present our conclusions in Section 4.

2 SAMPLE

The SDSS DR7 covers an imaging area of about 11 663 deg^2 and a spectroscopic area of about 9380 deg^2 (Abazajian et al. 2009). Schneider et al. (2010) have presented a quasar catalogue from the SDSS DR7, consisting of 105 783 QSOs with $M_i < -22$, an increase of 30 per cent with respect to the number in DR5. The wavelength coverage of the SDSS spectrum is 3800–9200 Å. In order to investigate the C IV line, we have selected 51 523 QSOs with $z \geq 1.5$ from the SDSS DR7 QSOs.

Shen et al. (2011) have carefully considered the ultraviolet/optical Fe II contribution, the host contribution in low-redshift (low-z) QSOs and a multiple-Gaussian fit for four lines of Hα, Hβ, Mg II and C IV for the calculation of the single-epoch virial SMBH mass. In their SDSS spectral analysis, they have removed the effects of Galactic extinction in the SDSS spectra, and have shifted the spectra to the rest frame. As well as these continuum and line properties, they have also compiled the radio, infrared and X-ray properties (Schneider et al. 2010).

Because the properties of the rest-frame C IV EW, $M_{\rm BH}$ and $L_{\rm Bol}/L_{\rm Edd}$ have been adopted by Shen et al. (2011), we briefly describe their spectral analysis. Because of the weakness of Fe II and the signal-to-noise (S/N) ratio of the C IV line was not high enough, Shen et al. (2011) have only reported their C IV measurements without the Fe II template fits. They have emphasized that their C IV EWs might be overestimated by 0.05 dex, on average. They have performed fits for the C IV line over the [1500 Å, 1600 Å] wavelength range, with multiple Gaussians. They have not subtracted the C IV narrow component (e.g. Sulentic et al. 2007). Considering the possible narrow or broad absorption features of the C IV line in high-z QSOs, they have masked out 3σ outliers below the 20 pixel boxcar-smoothed spectrum during the fits for the narrow absorption. They have performed a second fit, excluding pixels below 3σ of the first model fit for the broad absorption. They have given the broad absorption line (BAL) flag for the SDSS DR7 QSOs. The QSOs flagged as BAL QSOs are not used in our investigation of the Baldwin effect.

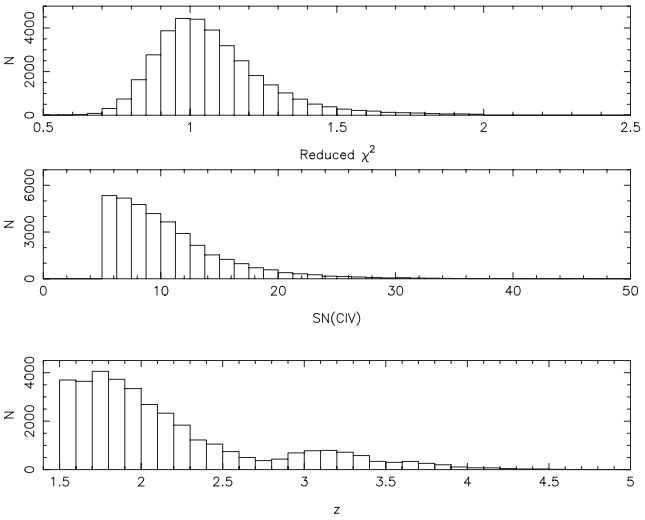

Figure 1. Distributions of the redshift z, S/N ratio (C IV) and reduced χ^2.

For QSOs with $1.5 \leq z \leq 2.25$, they have also fitted the Mg II emission line, as well as the SMBH mass from the Mg II line. They have obtained a fit for the Mg II line over the [2700 Å, 2900 Å] wavelength range, using a single Gaussian (with FWHM < 1200 km s^{-1}) for the narrow component, and for the broad component with a single Gaussian or multiple Gaussians. They have provided a new mass calibration from the Mg II lines using their multiple-Gaussian fits with narrow-line subtraction, which is adopted as the fiducial virial SMBH mass for QSOs with $0.9 \leq z < 1.9$. For $z \geq 1.9$, they have adopted the equations of Vestergaard & Peterson (2006) to calculate the C IV virial mass.

We use the following criteria to select our sample: $z \geq 1.5$, FWHM(C IV) > 1200 km s^{-1}, reduced $\chi^2 < 2.0$, EW(C IV) > 2.0, SN(C IV) > 5, excluding BAL QSOs. Our sample contains 35 019 QSOs (∼68 per cent of 51 523 QSOs). The distributions of redshift, S/N ratio and reduced χ^2 are shown in Fig. 1. For the SMBH mass, we have adopted the fiducial viral masses from Mg II for $z < 1.9$ and the masses from C IV for $z > 1.9$, for which the numbers of QSOs are 14 652 and 19 476, respectively (Shen et al. 2011). Xu et al. (2008) used 26 623 QSOs to investigate the C IV Baldwin effect, and 13 960 QSOs to investigate the relation of the C IV EW to the accretion parameters ($M_{\rm BH}$, $L_{\rm Bol}/L_{\rm Edd}$).

3 RESULTS AND DISCUSSION

3.1 Relation between the rest-frame C IV EW and L_{1350}

The following equation is used to express the relation between the C IV EW and the continuum luminosity at 1350 Å (L_{1350}):

$$\log {\rm EW(C\,IV)} = \alpha + \beta \log L_{1350}. \quad (1)$$

Fig. 2 gives the relation between the C IV EW and L_{1350} for 35 019 QSOs from the SDSS DR7. For the total of 35 019 QSOs, the Spearman's rank correlation coefficient is $R = -0.33$ and the null hypothesis is less than 10^{-4}.

The regression analyses are performed using the bivariate correlated errors and intrinsic scatter (BCES) algorithm (Akritas & Bershady 1996). There is some difference between the BCES($Y|X$) [i.e. $Y = f(X)$] and BCES($X|Y$) [i.e. $X = g(Y)$] regressions. The bisector bisects these two regressions. The BCES regression is robust;

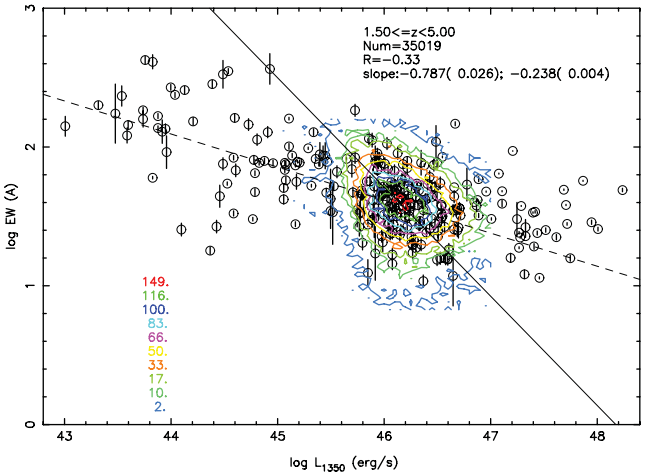

Figure 2. The log–log correlation between the C IV EW and the continuum luminosity at 1350 Å (in erg s^{-1}) for the SDSS DR7 sample of 35 019 QSOs with $1.5 \leq z < 5.0$. In the bottom-left corner, the numbers for the coloured contour levels are shown. The solid line is the linear fit from the BCES bisector and the bootstrap simulation. The dashed line is the BCES with EW(C IV) as the dependent variable and L_{1350} as the independent variable. In the top-right corner, we list the redshift coverage, the number of the sample, the Spearman's rank correlation coefficient and the slopes with BCES($Y|X$) and BCES bisector. Black circles denote data from a compiled sample of Wu et al. (2009).

bootstrapping simulations reproduce the theoretically expected results well (e.g. Akritas & Bershady 1996). For the SDSS sample, with the BCES($Y|X$) (X is L_{1350}), the slope is $\beta = -0.238 \pm 0.040$, and the intercept is $\alpha = 12.6 \pm 0.19$. However, with the BCES bisector, the slope is $\beta = -0.787 \pm 0.026$, and the intercept is $\alpha = 37.9 \pm 1.20$ (see Table 1).

In Fig. 2, we also plot the compiled sample from Wu et al. (2009). Their compiled sample consists of 272 AGNs: 189 from the SDSS, 47 from the *Hubble Space Telescope* and 36 from the *International Ultraviolet Explorer*. Wu et al. (2009) have used two Gaussian profiles to fit the C IV emission lines after subtracting the power-law continuum. The continuum luminosity at the rest-frame 2500 Å in Wu et al. (2009) is converted to the luminosity at the rest-frame 1350 Å by assuming $f_\nu \propto \nu^{-0.44}$ (i.e. larger by ∼0.12 dex; Vanden Berk et al. 2001). In Fig. 2, the data of Wu et al. (2009) are consistent with our SDSS DR7 sample, as well as the dashed line from BCES($Y|X$). For the compiled sample of Wu et al. (2009), there are 163 common QSOs in our SDSS DR7 sample. For these 163 common QSOs, the C IV EWs from Wu et al. (2009) are very consistent with those from Shen et al. (2011); the C IV EW ratio has a normal distribution with mean 0.01 and dispersion 0.12.

For 81 PG QSOs from Baskin & Laor (2004), for 454 Large Bright Quasar Survey objects from Forster et al. (2001) and for 125 pre-COSTAR AGNs from Kuraszkiewicz et al. (2002), we find that these QSOs/AGNs are also located in the region of the SDSS QSOs or that they are consistent with the dashed line from BCES($Y|X$) if they are scaled to our Fig. 2.

The Baldwin effect provides a potential method to infer the luminosity of a QSO from its C IV observation. With respect to classical standard candles of Type Ia supernovae (SNe), QSOs can be observed to a much higher redshift. For our SDSS DR7 sample, we find the relation between L_{1350} and the rest-frame C IV EW using BCES ($Y|X$) and the BCES bisector, respectively:

$$\log L_{1350} = (-0.511 \pm 0.042) \log \mathrm{EW(C\,IV)} + (46.977 \pm 0.066);$$

$$\log L_{1350} = (-1.271 \pm 0.043) \log \mathrm{EW(C\,IV)} + (48.179 \pm 0.068).$$

Table 1. The C IV EW and the continuum luminosity regression parameters: $\log \mathrm{EW(C\,IV)} = \alpha + \beta \log \mathrm{L_{1350}}$.

z (1)	No. (2)	R (3)	β^a (4)	α^a (5)	β^b (6)	α^b (7)	$P_{\rm null}$ (8)
SDSS DR7 sample							
1.5–5.0	35 019	−0.33	-0.238 ± 0.040	12.6 ± 0.19	-0.787 ± 0.026	37.9 ± 1.20	1.15×10^{-25}
SDSS DR7 sample in different z bins							
1.5–1.6	3699	−0.33	-0.386 ± 0.021	19.4 ± 0.98	-1.065 ± 0.015	50.2 ± 0.70	3.90×10^{-4}
1.6–1.7	3645	−0.32	-0.292 ± 0.016	15.0 ± 0.75	-0.911 ± 0.020	43.5 ± 0.93	8.93×10^{-4}
1.7–1.8	3727	−0.35	-0.283 ± 0.013	14.6 ± 0.58	-0.887 ± 0.014	42.4 ± 0.63	2.65×10^{-5}
1.8–1.9	4057	−0.35	-0.272 ± 0.012	14.1 ± 0.57	-0.845 ± 0.014	40.5 ± 0.65	5.29×10^{-5}
1.9–2.0	3343	−0.31	-0.233 ± 0.013	12.3 ± 0.60	-0.830 ± 0.014	39.9 ± 0.63	2.73×10^{-3}
2.0–2.1	2687	−0.32	-0.230 ± 0.015	12.2 ± 0.70	-0.858 ± 0.015	41.2 ± 0.67	6.10×10^{-3}
2.1–2.25	3265	−0.33	-0.249 ± 0.013	13.1 ± 0.62	-0.850 ± 0.016	40.9 ± 0.74	1.32×10^{-3}
2.25–2.5	3173	−0.34	-0.273 ± 0.014	14.2 ± 0.64	-0.840 ± 0.015	40.4 ± 0.67	4.99×10^{-4}
2.5–3.0	2740	−0.34	-0.279 ± 0.015	14.5 ± 0.69	-0.845 ± 0.023	40.7 ± 1.06	9.22×10^{-4}
3.0–3.5	3213	−0.30	-0.238 ± 0.014	12.6 ± 0.66	-0.698 ± 0.242	33.9 ± 11.2	7.52×10^{-3}
3.5–5.0	1470	−0.27	-0.215 ± 0.022	11.5 ± 1.04	-0.031 ± 0.696	2.93 ± 32.4	1.59×10^{-1}
SDSS DR7 sample in different z bins ($10^{45.6} \leq L_{1350} \leq 10^{46.6}$ erg s^{-1})							
1.5–1.6	3566	−0.30	-0.387 ± 0.023	19.4 ± 1.05	-1.140 ± 0.015	53.8 ± 0.70	4.74×10^{-3}
1.6–1.7	3474	−0.28	-0.293 ± 0.018	14.9 ± 0.83	-0.997 ± 0.018	47.5 ± 0.81	1.43×10^{-2}
1.7–1.8	3836	−0.31	-0.287 ± 0.016	14.7 ± 0.74	-0.919 ± 0.012	44.1 ± 0.55	1.41×10^{-3}
1.8–1.9	3518	−0.31	-0.280 ± 0.016	14.5 ± 0.73	-0.882 ± 0.052	37.6 ± 0.24	3.52×10^{-3}
1.9–2.0	3136	−0.27	-0.230 ± 0.016	12.2 ± 0.75	-0.828 ± 0.011	38.9 ± 0.53	3.48×10^{-2}

[a]BCES($Y|X$) where Y is EW(C IV) as the dependent variable and X is L_{1350} as the independent variable.
[b]The BCES bisector result.

From the above equations, we can calculate the rms values of the residuals after subtracting the predicted luminosity from the measured C IV EW. We find that they are 0.286 and 0.345, respectively. In order to use QSOs as standard candles via the Baldwin effect, it is suggested that we should at least confine the luminosity within an uncertainty of 30 per cent, ∼0.13 dex (Wu et al. 2009). Therefore, it is impossible to use the QSOs of our data set as standard candles via the Baldwin effect.

3.2 Slope of the Baldwin effect

In previous studies, the slope of the Baldwin effect has been found to be $-0.14 \sim -0.20$ (see table 1 in Xu et al. 2008, and references therein). Dietrich et al. (2002) have found that the slope becomes steep for luminous QSOs, from −0.14 for their total sample to −0.20 for QSOs with $\log \lambda L_\lambda(1450\ \text{Å}) \geq 44$ erg s^{-1}. We obtain a slope from the BCES($Y|X$), $\beta = -0.238 \pm 0.04$ (Table 1), which is steeper than in some previous studies. Using the BCES bisector, the slope is $\beta = -0.787 \pm 0.026$. The slope of the BCES bisector (−0.787) is more consistent with the slope of the 'intrinsic' Baldwin effect ($\beta = -0.72$) from Pogge & Peterson (1992). Considering the compiled sample of Wu et al. (2009), the slope from the BCES($Y|X$) is better than the slope of the BCES bisector when a wide luminosity range for QSOs is considered (Fig. 2).

The redshift coverage of our sample is from 1.5 to 5.0 (see Fig. 1). In order to investigate the relation of the Baldwin effect with the redshift, we divide our sample into 11 bins according to the redshift. These redshift bins are 1.5–1.6, 1.6–1.7, 1.7–1.8, 1.8–1.9, 1.9–2.0, 2.0–2.1, 2.1–2.25, 2.25–2.5, 2.5–3.0, 3.0–3.5 and 3.5–5.0 (see Table 1). The number in each different redshift bin is about 3000. For different redshift bins, we calculate the Spearman's rank correlation coefficient, the null possibility, the slopes and the intercepts with the BCES ($Y|X$) and the BCES bisector (Table 1). Except for the highest bin ($3.5 \leq z < 5.0$), we find a medium strong correlation for different redshift bins ($|R| \geq 0.3$).

It seems that there is an increase of the slope from $z \sim 1.5$ to $z \sim 2$ (Fig. 3), which is the same as that by the BCES ($Y|X$) and the BCES bisector. From $z \sim 2$ to $z \sim 5$, the slope evolution is not clear because of the large uncertainties. If we believe that the Baldwin effect is a result of the softening of the SED for increasing

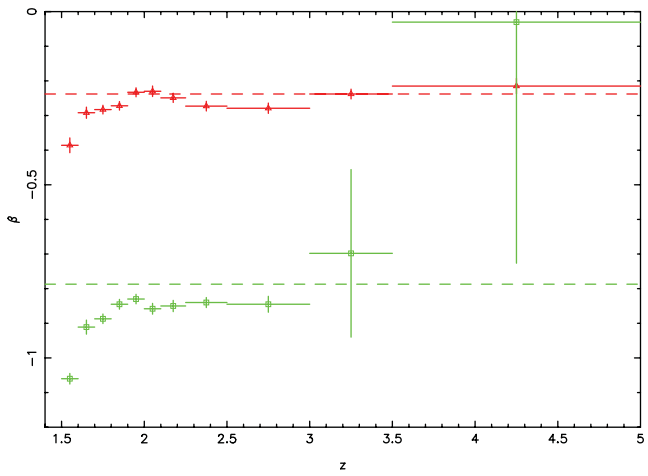

Figure 3. The slope versus the redshift. The red points are for the slopes by the BCES($Y|X$). The green points are for the slopes by the BCES bisector. The red and green dashed lines are for the slopes for the total sample, using the BCES($Y|X$) and bisector, respectively.

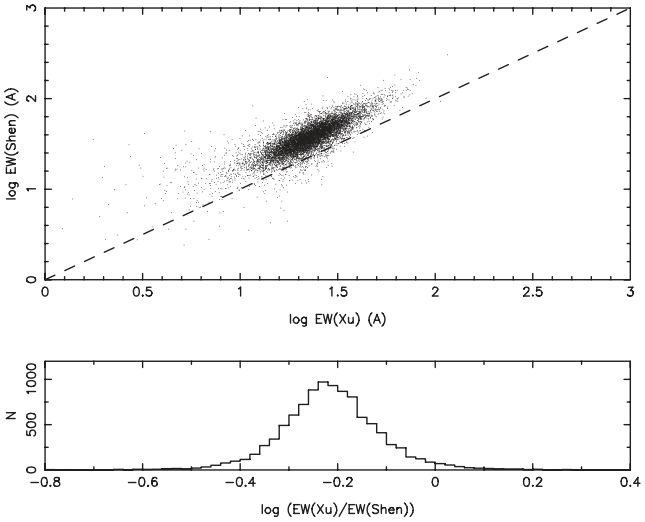

Figure 4. Top: A comparison of the rest-frame C IV EW for 10 232 common QSOs from the current sample and from Xu et al. (2008). The dashed line is 1: 1. Bottom: the distribution of the EW ratio of QSOs from Xu et al. (2008) to the current sample.

luminosity, the slope evolution from $z \sim 1.5$ to $z \sim 2$ implies the evolution of the QSO SED below $z \sim 2$. This is also possibly related to the covering factor evolution. In low-redshift bins, the dynamical range in luminosity is larger because of the flux-limited nature of the sample, which might affect the linear regression. For redshift bins below $z = 2.0$, in the same luminosity range (i.e. $10^{45.6}$–$10^{46.6}$ erg s^{-1}), we find that $R \sim -0.3$, and the slopes are consistent with the results for the total sample in different redshift bins (Table 1).

Using the SDSS DR5, Xu et al. (2008) used the SpecLine table to investigate the C IV Baldwin effect. The SpecLine table is from the pipeline of the SDSS spectral fit. The C IV line feature is measured by a single Gaussian fit for the continuum-subtracted spectrum. Xu et al. (2008) investigated the C IV Baldwin effect in the observed frame. In Xu et al. (2008), there was no correction of Galactic extinction for L_{1350} and the C IV EW was given in the observed frame. In Fig. 4, we show a comparison of the C IV EW in the rest frame for 10 232 common QSOs from the current sample and from Xu et al. (2008). We find that the rest-frame C IV EW from the current sample is, on average, larger by 0.23 dex than that from Xu et al. (2008). The difference is because of the spectral fitting, such as a single Gaussian fit for C IV in Xu et al. (2008) and a multiple-Gaussian fit in Shen et al. (2011).

3.3 Relation between the C IV EW and $M_{\rm BH}$ or $L_{\rm Bol}/L_{\rm Edd}$

The underlying physical origin for the Baldwin effect is still an open question. The fundamental process in QSOs is the accretion around the SMBH. Using the data from Shen et al. (2011), we also investigate the relation between the rest-frame C IV EW and $M_{\rm BH}$ or $L_{\rm Bol}/L_{\rm Edd}$ (Fig. 5). For the total sample, we find a medium strong correlation between the rest-frame C IV EW and $M_{\rm BH}$ with $R = -0.27$, and the null hypothesis is less than 10^{-4}. However, the correlation between the C IV EW and $L_{\rm Bol}/L_{\rm Edd}$ is very weak, $R = 0.01$ (Fig. 5). Earlier studies on individual sources suggest that for the same object, an intrinsic Baldwin effect does exist (albeit with a different slope). Therefore, luminosity does drive the Baldwin effect (for the same object, this is the same as saying that $L_{\rm Bol}/L_{\rm Edd}$ drives the Baldwin effect). We find that the very weak correlation between the C IV EW and $L_{\rm Bol}/L_{\rm Edd}$ for the total SDSS DR7 sample

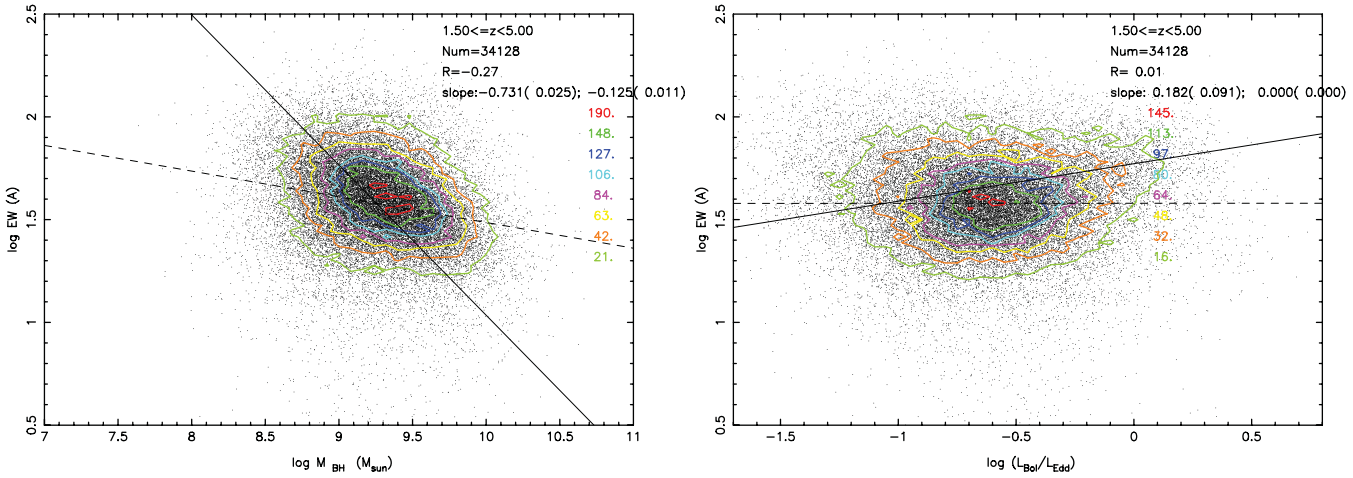

Figure 5. The log–log correlation between the rest-frame C IV EW and $M_{\rm BH}$ (left) and $L_{\rm Bol}/L_{\rm Edd}$ (right). On the right in each panel, the numbers for the coloured contour levels are shown. The solid line is the linear fit from the BCES bisector and the bootstrap simulation. The dashed line is BCES with EW(C IV) as the dependent variable and $M_{\rm BH}/L_{\rm Bol}/L_{\rm Edd}$ as the independent variable. In the top-right corner, we list the redshift coverage, the number of the sample, the Spearman's rank correlation coefficient, the slopes and their errors with BCES($Y|X$) and BCES bisector.

is a result of the mixed use of Mg II-based and C IV-based estimates of $M_{\rm BH}$.

For QSOs with $z \geq 1.9$, we use the mass from the C IV line, while we use the mass from the Mg II line for QSOs with $1.5 \leq z < 1.9$ (Shen et al. 2011). So, we divide our total sample into two samples: $1.5 \leq z < 1.9$ and $z \geq 1.9$. For QSOs with $1.5 \leq z < 1.9$, we find a very weak correlation of $R = 0.07$ between the rest-frame C IV EW and the mass from the Mg II line. For the physical driver of the Baldwin effect, L_{1350} and $M_{\rm BH}$ are two essentially independent quantities. To understand which is a better physical driver of the Baldwin effect, we need to look at them separately (i.e. at fixed L_{1350} or fixed $M_{\rm BH}$). Using the whole sample with mixed $M_{\rm BH}$ and L_{1350} makes it difficult to isolate the two. For L_{1350} between $10^{45.7}$ and $10^{46.5}$ erg s^{-1}, we divide the total SDSS sample into four luminosity bins ($\Delta \log L_{1350} = 0.2$), and we find that this correlation between the C IV EW and $M_{\rm BH}$ is stronger ($R \sim 0.18$) than that for the total SDSS sample ($R \sim 0.07$). For QSOs with $z \geq 1.9$, we find a strong correlation of $R = -0.48$ between the C IV EW and C IV-based $M_{\rm BH}$ (see Table 2 and Fig. 6). This is consistent with our previous result, where we used the C IV FWHM from the standard pipeline of the SDSS to calculate the single-epoch $M_{\rm BH}$ (Vestergaard & Peterson 2006; Xu et al. 2008). In Section 3.4, we discuss the bias in C IV-based $M_{\rm BH}$.

For QSOs with $1.5 \leq z < 1.9$, we find a modest correlation between the C IV EW and $L_{\rm Bol}/L_{\rm Edd}$ ($R = -0.28$). Because the Mg II-based $M_{\rm BH}$ is proportional to $v^2 \times R_{\rm BLR}$, and $R_{\rm BLR} \propto L_{1350}^{0.62}$ (Shen et al. 2011), then $L_{\rm Bol}/L_{\rm Edd}$ is proportional to $L_{1350}^{0.38}$, neglecting the effect of the Mg II FWHM. We find that EW(C IV) $\propto (L_{\rm Bol}/L_{\rm Edd})^{-0.27}$ for QSOs with $1.5 \leq z < 1.9$ by BCES($Y|X$). Using this correlation, we can derive the expected Baldwin effect of EW(C IV) $\propto L_{1350}^{-0.10}$; however, the slope of the Baldwin effect (Table 1) is -0.24. This suggests that the relation between the C IV EW and $L_{\rm Bol}/L_{\rm Edd}$ is not completely derived from the relation between the C IV EW and L_{1350}. We use the partial Kendall τ to investigate the role of L_{1350} in the relation between the C IV EW and $L_{\rm Bol}/L_{\rm Edd}$ for the total sample. We find that the relation between the C IV EW and $L_{\rm Bol}/L_{\rm Edd}$ is weakened when L_{1350} is kept fixed. The partial Kendall τ is -0.135 for QSOs with $1.5 \leq z < 1.9$ and 0.097 for QSOs with $1.9 \leq z < 5.0$, while their Spearman's rank correlation coefficients are -0.28 and 0.26, respectively (Table 2). It is possible that $L_{\rm Bol}/L_{\rm Edd}$ is not very important in controlling the Baldwin effect, or that the large uncertainty of individual $M_{\rm BH}$ estimates is diluting any inherent correlation.

Fig. 6 also shows the location of low-z PG QSOs from Baskin & Laor (2004), where $M_{\rm BH}$ was calculated from the Hβ FWHM. These PG QSOs, which are denoted by black circles in Fig. 6, are very consistent with our sample of $1.5 \leq z < 1.9$ QSOs where Mg II-based $M_{\rm BH}$ is used. However, these PG QSOs do not follow the relation found for $1.9 \leq z < 5.0$ QSOs where the C IV-based $M_{\rm BH}$ is used. With respect to Hβ-based $L_{\rm Bol}/L_{\rm Edd}$, it was found that the relation between EW(C IV) and $L_{\rm Bol}/L_{\rm Edd}$ is weaker when $L_{\rm Bol}/L_{\rm Edd}$ is based on the C IV FWHM (Baskin & Laor 2005). Considering the strong correlation between the C IV EW and $L_{\rm Bol}/L_{\rm Edd}$ for low-z PG QSOs found by Baskin & Laor (2004), our result also shows a strong bias of C IV-based $M_{\rm BH}$, with respect to Mg II-based $M_{\rm BH}$.

3.4 C IV-based $M_{\rm BH}$ correction from the C IV blueshift relative to Mg II

We should keep in mind that the analysis of the underlying physical drive depends on the calculation of $M_{\rm BH}$. The bias of $M_{\rm BH}$ calculated from Mg II and C IV has been investigated (e.g. Rafiee & Hall 2011; Shen & Liu 2012). It is found that the C IV-based $M_{\rm BH}$ is biased to the possible non-virialized component in C IV (Shen et al. 2008; Richards et al. 2011; Shen et al. 2011; Shen & Liu 2012). The Mg II-based $M_{\rm BH}$ can be calibrated to yield consistent virial mass estimates with those based on Hα/Hβ, while the C IV-based $M_{\rm BH}$ is poorly correlated with the Hβ-based $M_{\rm BH}$ or Hα-based $M_{\rm BH}$ (Shen & Liu 2012). It was found that the C IV blueshift relative to Hβ can be used as a C IV FWHM correction (Shen & Liu 2012). For 24 228 QSOs with $1.5 \leq z \leq 2.25$, we find a strong correlation between C IV-based $M_{\rm BH}$ and the C IV blueshift relative to Mg II ($\Delta V = v_{\rm off,C\,IV} - v_{\rm off,Mg\,II}$), $R = -0.41$. We also find a strong correlation between the C IV EW and the C IV blueshift relative to Mg II, $R = -0.38$ (bottom-left panel in Fig. 7; $R = -0.11$ when only using the C IV blueshift). This strong correlation between the C IV EW and the C IV blueshift relative to Mg II is consistent with the disc+wind model (Richards et al. 2011). It is possible that QSOs with larger C IV blueshift have softer SEDs and have a stronger wind component to dominate over the disc component.

Table 2. The C IV EW drive regression parameters: $\log \mathrm{EW(C\,IV)} = \alpha + \beta \log \mathrm{L_{1350}}$, $\log \mathrm{EW(C\,IV)} = \alpha + \beta \log \mathrm{M_{BH}}$ or $\log \mathrm{EW(C\,IV)} = \alpha + \beta \log \mathrm{L_{Bol}/L_{Edd}}$.

Drive (1)	z (2)	No. (3)	R (4)	β^a (5)	α^a (6)	β^b (7)	α^b (8)
L_{1350}	1.5–5.0	35 019	−0.33	-0.238 ± 0.040	12.6 ± 0.19	-0.787 ± 0.026	37.9 ± 1.20
	1.5–1.9	15 128	−0.34	-0.299 ± 0.076	15.4 ± 0.35	-0.920 ± 0.007	44.0 ± 0.34
	1.9–5.0	19 891	−0.31	-0.226 ± 0.051	12.0 ± 0.23	-0.755 ± 0.057	36.5 ± 2.63
$M_{\rm BH}$	1.5–5.0	34 128	−0.27	-0.125 ± 0.011	2.74 ± 0.10	-0.731 ± 0.025	8.34 ± 0.23
	1.5–1.9	14 652	0.07	0.665 ± 0.087	0.985 ± 0.08	0.959 ± 0.057	-7.22 ± 0.05
	1.9–5.0	19 476	−0.48	-0.178 ± 0.019	32.3 ± 0.18	-0.521 ± 0.052	6.41 ± 0.49
$L_{\rm Bol}/L_{\rm Edd}$	1.5–5.0	34 128	0.01	0.272 ± 0.001	1.58 ± 0.01	0.182 ± 0.091	1.77 ± 0.83
	1.5–1.9	14 652	−0.28	-0.268 ± 0.080	1.41 ± 0.06	-0.858 ± 0.080	0.992 ± 0.07
	1.9–5.0	19 476	0.26	0.0003 ± 0.00009	1.57 ± 0.01	0.090 ± 0.067	1.69 ± 0.07

[a]BCES($Y|X$) where Y is EW(C IV) as the dependent variable and X is L_{1350}, $M_{\rm BH}$ and $L_{\rm Bol}/L_{\rm Edd}$ as the independent variable, respectively.
[b]The BCES bisector result.

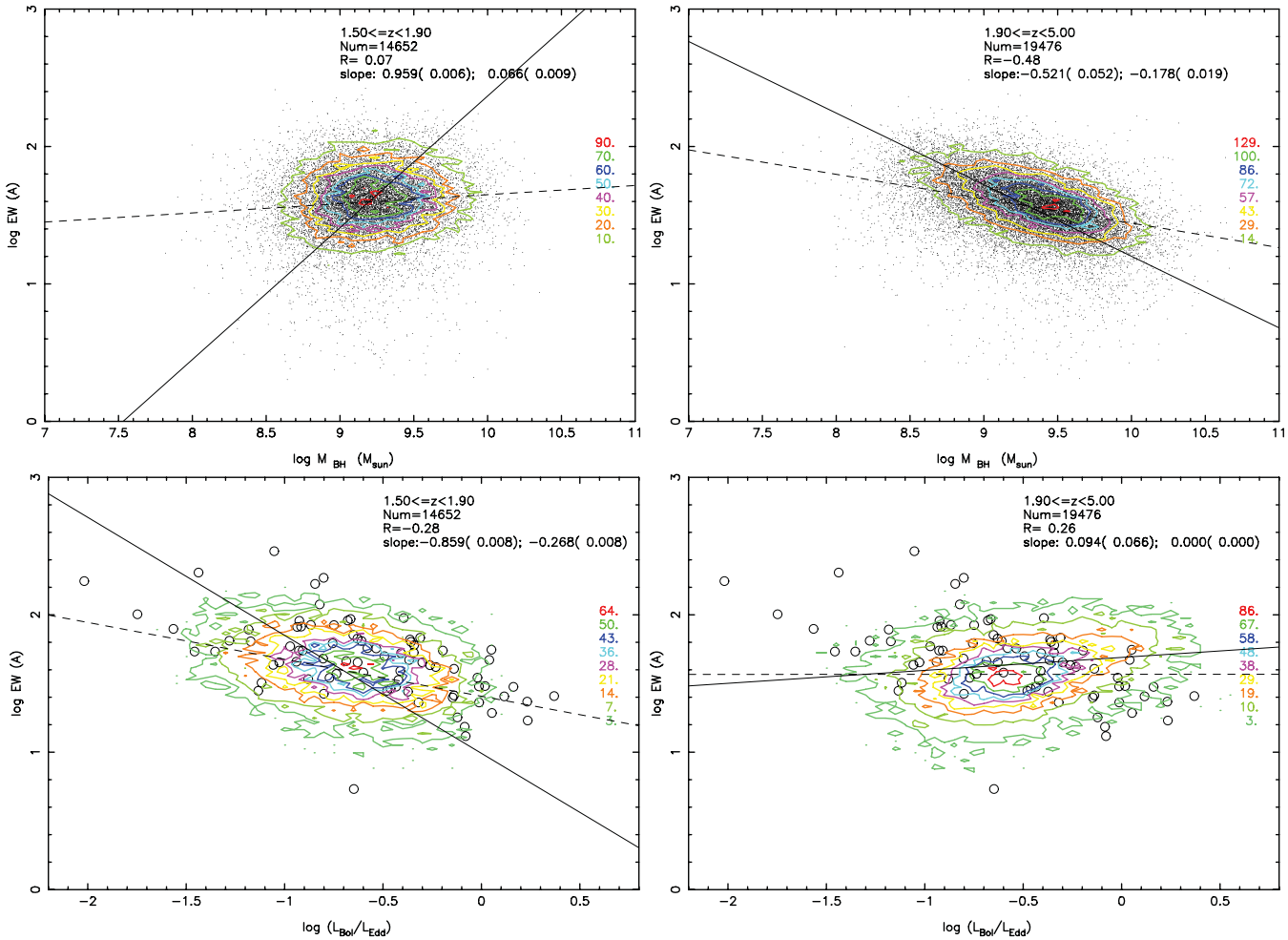

Figure 6. The log–log correlation between the rest-frame C IV EW and the $M_{\rm BH}$ (top) and $L_{\rm Bol}/L_{\rm Edd}$ (bottom) for two redshift bins: $1.50 \leq z < 1.9$ and $z \geq 1.9$. On the right in each panel, the numbers for the coloured contour levels are shown. The solid line is the linear fit from the BCES bisector and the bootstrap simulation. The dashed line is BCES with EW(C IV) as the dependent variable and $M_{\rm BH}/L_{\rm Bol}/L_{\rm Edd}$ as the independent variable. In the top-right corner of each panel, we list the redshift coverage, the number of the sample, the Spearman's rank correlation coefficient, the slopes and their errors with BCES($Y|X$) and BCES bisector. The black circles in the two bottom panels are data from Baskin & Laor (2004).

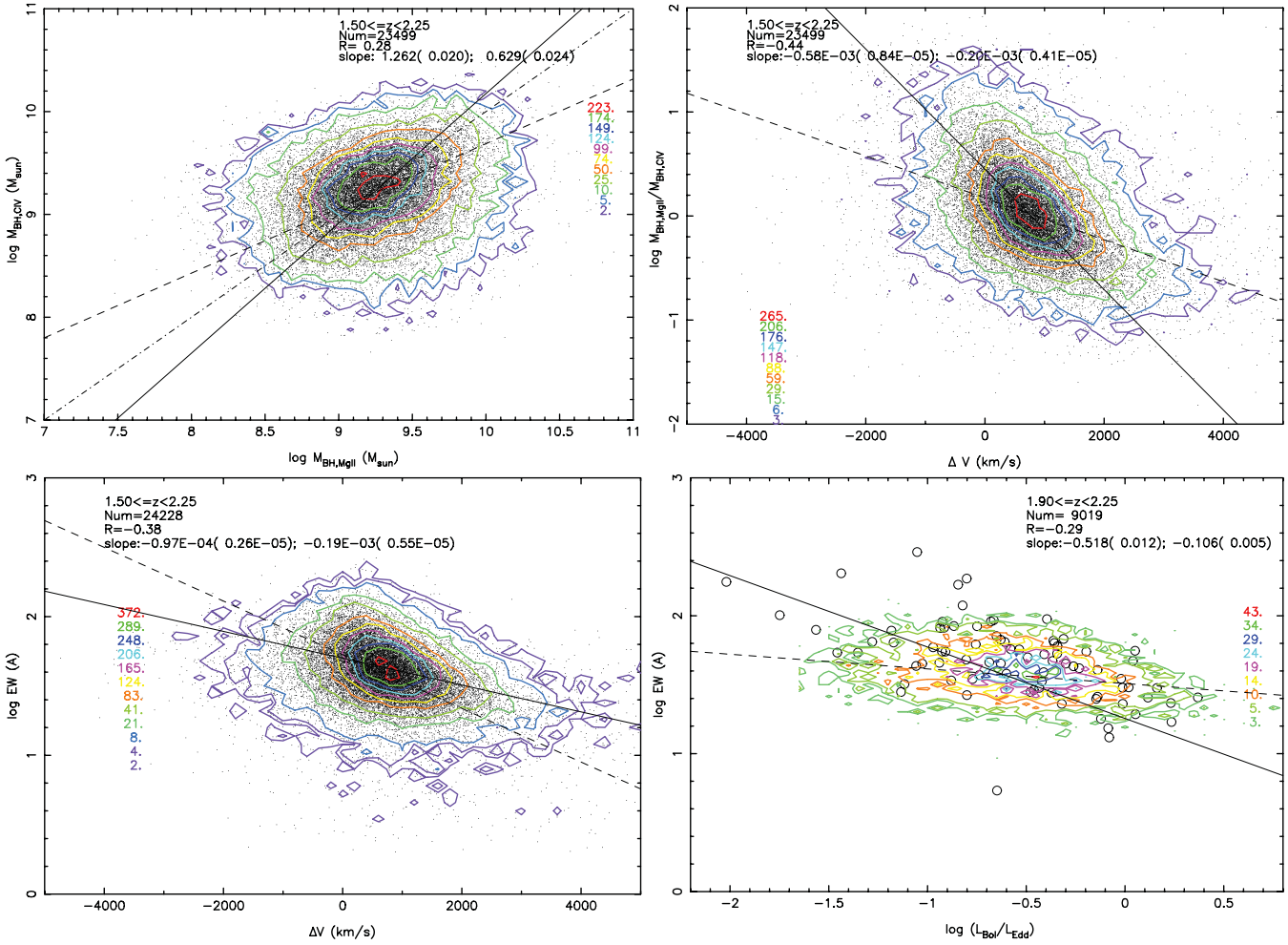

Figure 7. Top-left: C IV-based $M_{\rm BH}$ versus Mg II-based $M_{\rm BH}$. Top-right: the ratio of Mg II-based $M_{\rm BH}$ to C IV-based $M_{\rm BH}$ versus the C IV blueshift relative to Mg II. Bottom-left: the C IV EW versus the C IV blueshift relative to Mg II. Bottom-right: the C IV EW versus the corrected C IV-based $L_{\rm Bol}/L_{\rm Edd}$ (for clarity, the data points are not shown). The numbers for the coloured contour levels are shown in each panel. The solid line is the linear fit from the BCES bisector and the bootstrap simulation. The dashed line is BCES with Y as the dependent variable and X as the independent variable. In the top corner of each panel, we list the redshift coverage, the number of the sample, the Spearman's rank correlation coefficient, the slopes and their errors with BCES($Y|X$) and BCES bisector. The black circles in the bottom-right panel are data from Baskin & Laor (2004).

The C IV blueshift relative to Mg II would lead to the apparent correlation between the C IV EW and C IV-based $M_{\rm BH}$. We can use the C IV blueshift relative to Mg II to do the C IV-based $M_{\rm BH}$ correction. Shen et al. (2011) have given the Mg II-based $M_{\rm BH}$ and C IV-based $M_{\rm BH}$ for QSOs with $1.5 \leq z \leq 2.25$ (see their table 1). Their Spearman's rank correlation coefficient is $R = 0.28$ and the null hypothesis is less than 10^{-4} (top-left panel in Fig. 7). We use the C IV blueshift relative to Mg II to correct the C IV-based $M_{\rm BH}$. Using BCES regression analyses, we find a strong correlation between the $M_{\rm BH}$ difference ($\log M_{\rm BH,Mg\,II} - \log M_{\rm BH,Mg\,II}$) and the C IV blueshift relative to Mg II, $R = -0.44$ (top-right panel in Fig. 7):

$$\log M_{\rm BH,Mg\,II} - \log M_{\rm BH,C\,IV} = a + b(v_{\rm off,C\,IV} - v_{\rm off,Mg\,II}). \quad (2)$$

Here, $a = (0.174 \pm 0.004)$, $b = (-2.01 \pm 0.04) \times 10^{-4}$ using BCES($Y|X$), and $a = (0.449 \pm 0.007)$, $b = (-5.78 \pm 0.08) \times 10^{-4}$ using the BCES bisector.

Considering the correction of C IV-based $M_{\rm BH}$ using equation (2), the Spearman's rank correlation coefficient for the relation of the Mg II-based $M_{\rm BH}$ and the corrected C IV-based $M_{\rm BH}$ changes from 0.28 to 0.38 and 0.36, respectively. Using equation (2) with BCES($Y|X$) and BCES bisector to perform the C IV-based $M_{\rm BH}$ correction, we find that, for the relation between the C IV EW and $L_{\rm Bol}/L_{\rm Edd}$ for 9019 QSOs with $1.9 \leq z \leq 2.25$, R changes from 0.22 to -0.03 and -0.29, respectively (bottom-right panel). Also, for the relation between the C IV EW and the corrected C IV-based $M_{\rm BH}$, R changes from -0.45 to -0.24 and 0.1, respectively. These values are consistent with the results for 14 652 QSOs with $1.5 \leq z \leq 1.9$, where the Mg II-based $M_{\rm BH}$ is used.

3.5 Origin of the Baldwin effect

Considering the Mg II-based $M_{\rm BH}$ (QSOs with $z < 1.9$ QSOs), we find that the correlation coefficient for the relation between the C IV EW and L_{1350} ($R = -0.34$) is larger than for the other two relations (i.e. C IV EW versus $M_{\rm BH}$, C IV EW versus $L_{\rm Bol}/L_{\rm Edd}$; $R = 0.07$ and -0.28). Also, the correlation coefficient of the C IV EW with $L_{\rm Bol}/L_{\rm Edd}$ ($R = -0.28$) is larger than that of the C IV EW with $M_{\rm BH}$ ($R = 0.07$). This is consistent with the result by Baskin & Laor (2004). The stronger correlation between the C IV EW and $M_{\rm BH}$ in Xu et al. (2008) is because of the use of the C IV-based $M_{\rm BH}$. Therefore, using the larger sample, we find that the C IV EW is

primarily controlled by L_{1350}, with respect to $L_{\rm Bol}/L_{\rm Edd}$ and $M_{\rm BH}$. The modest correlation between the C IV EW and $L_{\rm Bol}/L_{\rm Edd}$ (larger than that between the C IV EW and $M_{\rm BH}$) implies that $L_{\rm Bol}/L_{\rm Edd}$ seems to be a better underlying physical parameter than $M_{\rm BH}$. The strong correlation between the C IV EW and C IV blueshift relative to Mg II gives support to the disc+wind model (e.g. Richards et al. 2011). The QSOs with larger C IV blueshift have softer SEDs and have a stronger wind component to dominate over the disc component.

4 CONCLUSIONS

With reference to our previous analysis for SDSS DR5 QSOs, we have used the SDSS DR7 QSO catalogue of Shen et al. (2011) to reinvestigate the Baldwin effect, its slope evolution and the underlying drive. The main conclusions can be summarized as follows.

(i) The Baldwin effect exists in the large sample of 35 019 QSOs with reliable spectral analysis. The correlation coefficient is $R = -0.33$, which is almost the same for QSOs in different redshifts, up to $z \sim 5$.

(ii) For the total sample, the slope is -0.238 using the BCES (the C IV EW depends on L_{1350}) and -0.787 using the BCES bisector.

(iii) For 11 redshift bins, there is an increase in the slope of the Baldwin effect from $z \sim 1.5$ to $z \sim 2.0$. From $z \sim 2.0$ to $z \sim 5.0$, the slope change is not clear, considering the uncertainties or the larger redshift bin.

(iv) Using 34 128 QSOs with $M_{\rm BH}$ and $L_{\rm Bol}/L_{\rm Edd}$ carefully derived from spectral decomposition by Shen et al. (2011), we find that there is a strong correlation between the rest-frame C IV EW and C IV-based $M_{\rm BH}$ for $1.9 \leq z < 5.0$ ($R = -0.48$). However, the relation between the C IV EW and Mg II-based $M_{\rm BH}$ for $1.5 \leq z < 1.9$ is very weak ($R = 0.07$). We think this is a result of the bias of the C IV-based $M_{\rm BH}$, with respect to the Mg II-based $M_{\rm BH}$. Using the correction of C IV-based $M_{\rm BH}$ from the C IV blueshift relative to Mg II, we find that the correlation of the C IV EW with corrected C IV-based $M_{\rm BH}$ becomes weak (from $R = -0.45$ to $R = 0.1$). Considering the Mg II-based $M_{\rm BH}$, a medium strong correlation is found between the C IV EW and $L_{\rm Bol}/L_{\rm Edd}$ ($R = -0.28$), which implies that $L_{\rm Bol}/L_{\rm Edd}$ seems to be a better underlying physical parameter than $M_{\rm BH}$.

ACKNOWLEDGMENTS

We are grateful for a discussion that was held during the LAMOST science meeting in 2012 April. We thank an anonymous referee for suggestions that have led to improvements in this paper. This work has been supported by the National Basic Research Programme of China – The 973 Programme (grant 2009CB824800), and the National Science Foundations of China (Nos. 11173016 and 11233003).

REFERENCES

Abazajian K. N. et al., 2009, ApJS, 182, 543
Akritas M. G., Bershady M. A., 1996, ApJ, 470, 706
Baldwin J. A., 1977, ApJ, 214, 679
Baskin A., Laor A., 2004, MNRAS, 350, L31
Baskin A., Laor A., 2005, MNRAS, 356, 1029
Bian W., Zhao Y., 2004, MNRAS, 347, 607
Dietrich M., Hamann F., Shields J. C., Constantin A., Vestergaard M., Chaffee F., Foltz C. B., Junkkarinen V. T., 2002, ApJ, 581, 912
Forster K., Green P. J., Aldcroft T. L., Vestergaard M., Foltz C. B., Hewett P. C., 2001, ApJS, 134, 35
Kaspi S., Smith P. S., Netzer H., Maoz D., Jannuzi B. T., Giveon U., 2000, ApJ, 533, 631
Kong M. Z., Wu X. -B., Wang R., Liu F. K., Han J. L., 2006, A&A, 456, 473
Kuraszkiewicz J. K., Green P. J., Forster K., Aldcroft T. L., Evans I. N., Koratkar A., 2002, ApJS, 143, 257
Netzer H., Laor A., Gondhalekar P. M., 1992, MNRAS, 254, 15
Netzer H., Mainieri V., Rosati P., Trakhtenbrot B., 2006, A&A, 453, 525
Nikolajuk M., Walter R., 2012, MNRAS, 420, 2518
Pogge R. W., Peterson B. M., 1992, AJ, 103, 1084
Rafiee A., Hall P. B., 2011, MNRAS, 415, 2932
Richards G. T. et al., 2006, ApJS, 166, 470
Richards G. T. et al., 2011, AJ, 141, 167
Schneider D. P. et al., 2010, AJ, 139, 2360
Shang Z. et al., 2003, ApJ, 586, 52
Shen Y., Liu X., 2012, ApJ, 753, 125
Shen Y., Greene J. E., Strauss M. A., Richards G. T., Schneider D. P., 2008, ApJ, 680, 169
Shen Y. et al., 2011, ApJS, 194, 45
Shields J. C., 2007, in Ho L. C., Wang J-M., eds, ASP Conf. Ser. Vol. 373, The Central Engine of Active Galactic Nuclei. Astron. Soc. Pac., San Francisco, p. 355
Sulentic J. W., Bachev R., Marziani P., Negrete C. A., Dultzin D., 2007, ApJ, 666, 757
Vanden Berk D. E. et al., 2001, AJ, 122, 549
Vestergaard M., Peterson B. M., 2006, ApJ, 641, 689
Warner C., Hamann F., Dietrich M., 2004, ApJ, 608, 136
Wu J., Vanden Berk D. E., Brandt W. N., Schneider D. P., Gibson R. R., Wu J., 2009, ApJ, 702, 767
Xu Y., Bian W. H., Yuan Q. R., Huang K., L., 2008, MNRAS, 389, 1703
Zhou X-L., Wang J. -M., 2005, ApJ, 618, L83

This paper has been typeset from a TEX/LATEX file prepared by the author.